

Sheaf Diffusion with Adaptive Local Structure for Spatio-Temporal Forecasting

Abeer Mostafa¹, Raneen Younis^{1, 2} and Zahra Ahmadi^{1, 2}

¹Peter L. Reichertz Institute for Medical Informatics, Hannover Medical School, Hannover, Germany

²Lower Saxony Center for Artificial Intelligence and Causal Methods in Medicine (CAIMed), Hannover, Germany

Abstract. Spatio-temporal systems often exhibit highly heterogeneous and non-intuitive responses to localized disruptions, limiting the effectiveness of conventional message passing approaches in modeling higher-order interactions under local heterogeneity. This paper reformulates spatio-temporal forecasting as the problem of learning information flow over locally structured spaces, rather than propagating globally aligned node representations. We introduce a spatio-temporal sheaf diffusion graph neural network (ST-Sheaf GNN) that embeds graph topology into sheaf-theoretic vector spaces connected by learned linear restriction maps. Unlike prior work that relies on static or globally shared transformations, our model learns dynamic restriction maps that evolve over time and adapt to local spatio-temporal patterns to enable substantially more expressive interactions. By explicitly modeling latent local structure, the proposed framework efficiently mitigates the oversmoothing phenomenon in deep GNN architectures. We evaluate our framework on a diverse set of real-world spatio-temporal forecasting benchmarks spanning multiple domains. Experimental results demonstrate state-of-the-art performance, highlighting the effectiveness of sheaf-theoretic topological representations as a powerful foundation for spatio-temporal graph learning. The code is available at: <https://anonymous.4open.science/r/ST-SheafGNN-6523/>.

1 Introduction Spatio-temporal forecasting on graphs is a fundamental challenge in urban computing, environmental monitoring, and infrastructure management. Real-world spatio-temporal dynamics exhibit complex, non-stationary dependencies that often violate simple proximity-based modeling assumptions. For example, a traffic accident during rush hour may trigger cascading congestion across distant neighborhoods while nearby streets remain largely unaffected (Figure 1.1). This behavior illustrates a key limitation of conventional graph-based approaches: spatial adjacency alone is insufficient to capture the heterogeneous and dynamic interactions that govern real-world spatio-temporal systems [18, 1].

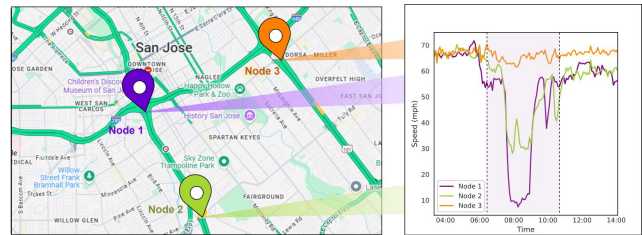


Figure 1.1: Spatio-temporal traffic dynamics across three sensor nodes in PEMS dataset [21]. Node 2 exhibits a strong temporal correlation with the significant speed drop at Node 1, whereas Node 3, despite similar spatial proximity, remains unaffected.

Recent spatio-temporal forecasting models combine graph neural networks [23, 27], attention mechanisms [10, 19], and diffusion models [29]. While effective in many settings, these methods primarily rely on fixed or uniformly weighted graph propagation and emphasize first-order spatial relationships or simplified temporal dependencies [23]. Such assumptions neglect the fact that interaction strength can vary significantly across space and time, often leading to oversmoothing and limiting the ability of such models to capture higher-order heterogeneous dependencies inherent in complex spatio-temporal systems. As a result, existing methods struggle to adaptively model how information propagates across different regions and time scales.

To address these limitations, we propose a novel spatio-temporal forecasting framework grounded in cellular sheaf theory [15], which generalizes graphs by associating vector spaces (stalks) with nodes and edges, and defining learnable linear maps (restriction maps) that govern information flow across the graph in a fully differentiable manner. Unlike static adjacency matrices, sheaf-based models enable *region-specific transformations*, allowing information to propagate differently across the graph (via learnable restriction maps), naturally preserving fine-grained spatial heterogeneity and

mitigating oversmoothing [3, 16]. The induced sheaf Laplacian generalizes the classical graph Laplacian to support multidimensional and higher-order interactions to be encoded through the underlying cellular structure. Building on this foundation, we further introduce *dynamic restriction maps* that evolve with spatio-temporal context. This design reframes spatio-temporal forecasting from aggregating neighbor features using fixed propagation rules to learning data-driven geometric operators that capture how local states co-evolve across the graph over space and time.

We evaluate our framework on six widely used benchmarks (METR-LA, PEMS04, PEMS08, NAVER-Seoul, Molene, AirQuality) across multiple prediction horizons and environmental settings. Experimental results demonstrate consistent improvements over state-of-the-art methods, highlighting the effectiveness and scalability of our approach for real-world applications such as transportation, environmental monitoring, and beyond.

Contributions. This work makes the following contributions:

- We propose the first dynamic sheaf-based formulation for spatio-temporal forecasting, modeling graph topology via *learned, locally heterogeneous restriction maps* that unifies heterogeneous spatial and temporal dynamics and effectively mitigates oversmoothing in deep GNN architectures.
- We design a *dynamic sheaf diffusion operator* that captures heterogeneous spatio-temporal interactions while remaining efficient and scalable.
- Extensive experiments across multiple domains demonstrate state-of-the-art performance and substantially improved expressive power compared to existing spatio-temporal GNN models.

2 Related Work *Spatio-temporal forecasting* has evolved through several architectural paradigms. Early approaches combined graph convolutions with sequential modeling to jointly capture spatial topology and temporal dynamics. STGCN [30] pioneered this direction by integrating spatial graph convolutions with temporal 1D convolutions in a unified framework, while DCRNN [21] modeled diffusion processes on directed graphs using gated recurrent units to capture asymmetric spatial dependencies. To overcome limitations of static adjacency matrices, subsequent work introduced adaptive graph learning: Graph WaveNet [28] that learns latent spatial dependencies directly from data through node embeddings. Subsequent work further refined adaptive graph learning through attention mechanisms to model dynamic, long-range dependencies. ASTGCN [13] employs spatial and temporal attention modules alongside graph convolutions for context-aware

feature weighting, while GMAN [32] introduces a graph multi-attention network with spatio-temporal positional encoding to capture complex interaction patterns across varying time horizons. More recently, SGP [7] achieves scalability via randomized recurrent architectures coupled with efficient spatial encodings. Spectral approaches have also emerged to model dynamics in the frequency domain. CITRUS [9] exploits the separability of continuous heat kernels on Cartesian graph products for efficient spectral decomposition, enabling modeling of multi-scale spatio-temporal patterns. The current state-of-the-art framework STDN [6] employs a trend-seasonality decomposition module that disentangles the trend-cyclical and seasonal components for each node at different times within the graph. Despite these advances, most methods remain constrained to first-order graph structures that assume uniform information propagation along edges, and nodes residing in the same space, limiting their ability to capture heterogeneous, higher-order dependencies, which motivates the move towards a different topological approach [4].

Sheaf graph neural networks: Recent research efforts have been presented to move beyond traditional spatial representations to capture higher-order interactions and address oversmoothing limitations in GNNs through sheaf theory [25, 5]. Sheaf neural networks represent a promising direction that applies concepts of algebraic topology to model asymmetric data relationships [14, 3]. Building on cellular sheaf theory, SheafANs [2] developed a sheaf attention mechanism that generalizes graph attention networks by integrating cellular sheaves for richer geometric inductive biases. This approach addresses the GNN limitations, oversmoothing, and poor performance on heterophilic graphs by using transport matrices and sheaf-based feature aggregation to preserve local heterogeneity and geometric structure. In [8], the authors introduce cellular sheaves for hypergraphs and propose the linear and non-linear sheaf hypergraph Laplacians, generalizing standard hypergraph Laplacians. Some gaps still exist in the research of sheaf graph neural networks, specifically the move from theoretical analysis or validation only on synthetic data [31] to benefit from it in reality. Our work employs the sheaf theory for modeling the asymmetric higher-order dependencies of real-world spatio-temporal systems.

3 The Proposed Framework Problem Definition: Let $\mathcal{G} = (\mathcal{V}, \mathcal{E})$ denote a graph with $N = |\mathcal{V}|$ nodes and $E = |\mathcal{E}|$ edges. We study a spatio-temporal forecasting problem where each node is associated with a multivariate time series. Given an observed historical window:

$$\mathbf{X} \in \mathbb{R}^{B \times T \times N \times F_{\text{in}}},$$

with batch size B , sequence length T , and input feature dimension F_{in} , the objective is to predict future node-level signals

$$\mathbf{Y} \in \mathbb{R}^{B \times H \times N \times F_{\text{out}}},$$

over a forecasting horizon H . Traditional graph neural networks assume that node features are expressed in a globally consistent latent space and that information propagates unchanged across edges. However, in many real-world systems, such assumptions are overly restrictive. This brings us to a common challenge of existing GNNs, which is oversmoothing, where node representations become increasingly similar and eventually indistinguishable as more layers are added. This occurs because repeated message passing causes features of neighboring nodes to converge, ultimately degrading the model’s ability to capture discriminative information. To address this issue and explicitly model such heterogeneity inherited in spatio-temporal data, we adopt a sheaf-theoretic formulation. The overall architecture is illustrated in Figure 3.1.

3.1 ST-Sheaf GNN

Temporal Encoding: To model temporal dependencies, we apply self-attention along the time dimension independently for each node. Let

$$\mathbf{Z}_v = [\mathbf{z}_{1,v}, \dots, \mathbf{z}_{T,v}] \in \mathbb{R}^{T \times D},$$

denote the embedded sequence for node v . A multi-head self-attention block computes:

$$(3.1) \quad \mathbf{Z}_v^{(1)} = \text{MHA}(\mathbf{Z}_v, \mathbf{Z}_v, \mathbf{Z}_v) + \mathbf{Z}_v,$$

where residual connections preserve the original signal. The output is further refined using layer normalization and a position-wise feed-forward network:

$$(3.2) \quad \begin{aligned} \mathbf{Z}_v^{(2)} &= \text{LayerNorm}(\mathbf{Z}_v^{(1)}), \\ \mathbf{Z}_v^{(3)} &= \text{FFN}(\mathbf{Z}_v^{(2)}) + \mathbf{Z}_v^{(2)}. \end{aligned}$$

Finally, the temporally encoded features are projected to a latent space that interfaces with subsequent spatial modeling:

$$(3.3) \quad \mathbf{h}_{t,v} = \mathbf{W}_{\text{proj}} \mathbf{z}_{t,v}^{(3)}, \quad \mathbf{h}_{t,v} \in \mathbb{R}^d,$$

where $\mathbf{W}_{\text{proj}} \in \mathbb{R}^{d \times D}$ is a learnable projection matrix. The sheaf diffusion will operate independently on each timestep $t \in \{1, \dots, T\}$. So for simplicity, we will denote $\mathbf{h}_u = \mathbf{h}_{t,u}$ when the timestep is clear from context.

Sheaf Building: Sheaves represent topological constructs that incorporate a lifting transformation applied to the input graph. This transformation elevates node attributes into an expanded, richer feature representation residing in a higher-dimensional space. Inspired by the sheaf definition in [14, 3], a cellular sheaf \mathcal{F} over \mathcal{G} assigns:

- a *vertex stalk* $\mathcal{F}(v) = \mathbb{R}^d$ to each node $v \in \mathcal{V}$,
- an *edge stalk* $\mathcal{F}(e) = \mathbb{R}^d$ to each edge $e \in \mathcal{E}$,
- linear *restriction maps*

$$\rho_{v \triangleleft e} : \mathcal{F}(v) \rightarrow \mathcal{F}(e), \quad \forall v \in e.$$

The vertex stalk represents a local latent coordinate system in which node-level signals are expressed. In contrast to standard GNNs, different nodes are not required to share a common representation space. Restriction maps align vertex representations to an edge space, enabling meaningful interaction between neighboring nodes with potentially different local coordinates. Figure 3.2 illustrates the new graph topology after sheaf associations.

An important hyperparameter in this setup is the stalk dimension d , which controls the capacity of the vector spaces. Higher-dimensional stalks support richer feature propagation and more informative graph signal encoding. When $d = 1$ and $\rho_{v \triangleleft e}$ is identity, we recover scalar-weighted message passing as in classical GCNs. We empirically analyze the impact of stalk dimensionality in the experiments section. We assume a uniform stalk dimension such that all vertex and edge stalks have identical dimension d , ensuring that $\mathcal{F}(v) \cong \mathcal{F}(e) \cong \mathbb{R}^d$ for all $v \in \mathcal{V}$ and $e \in \mathcal{E}$.

For an edge $e = (u, v)$, vertex-level representations are first aligned to the corresponding edge stalk through the restriction maps and become: $(\rho_{u \triangleleft e} \mathbf{h}_u), (\rho_{v \triangleleft e} \mathbf{h}_v)$.

These new representations lie in a shared edge-local coordinate system and enable comparison between node features that may otherwise live in different latent spaces.

This formulation allows us to design a different learning mechanism than the classical process in GNNs. Classical GNNs implicitly minimize an energy function that penalizes differences between neighboring node representations as:

$$(3.4) \quad \mathcal{E}(\mathbf{h}) = \frac{1}{2} \sum_{(u,v) \in \mathcal{E}} \|\mathbf{h}_u - \mathbf{h}_v\|_2^2.$$

Repeated minimization of this energy is also recognized as a primary cause of oversmoothing. This occurs because the energy function enforces global consistency: neighboring nodes must maintain similar representations regardless of their local structural or semantic context.

In contrast, the sheaf-based formulation relaxes this constraint by introducing learnable, edge-specific coordinate transformations. Rather than requiring direct agreement between \mathbf{h}_u and \mathbf{h}_v , we penalize disagreement only after aligning representations through restriction

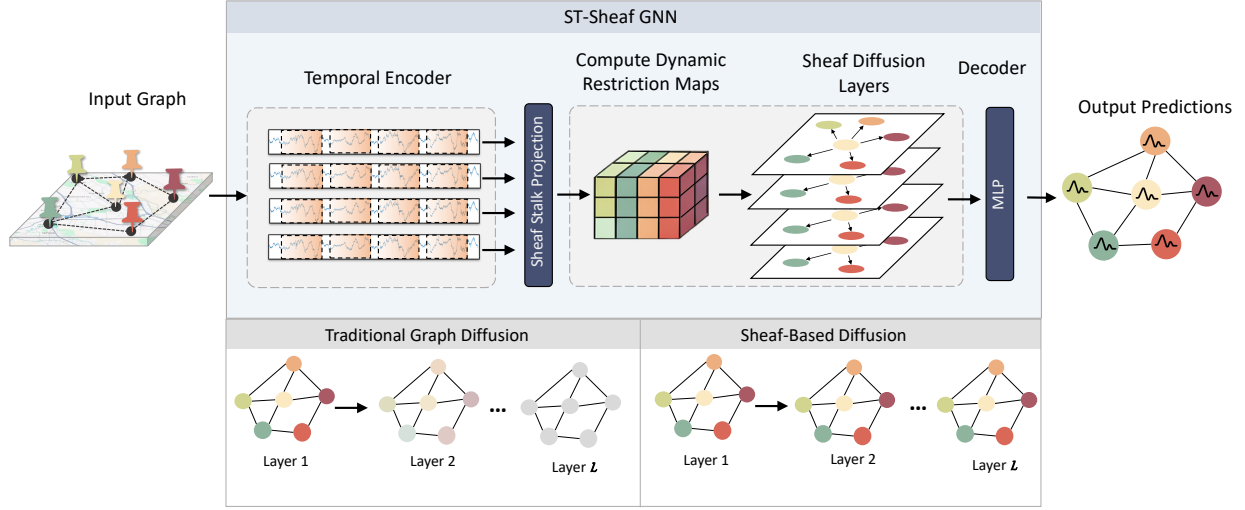


Figure 3.1: Overview of the proposed ST-Sheaf GNN. Multivariate time-series signals on a graph are first encoded with multi-head attention to capture temporal dependencies. The resulting representations are projected into a sheaf space, where dynamic restriction maps are computed. Sheaf diffusion layers propagate information by preserving local node distinct representation. The diffused features are finally decoded by an MLP to produce node-level forecasts.

maps. This yields a more expressive energy function:

$$(3.5) \quad \mathcal{E}_{\mathcal{F}}(\mathbf{h}) = \frac{1}{2} \sum_{e=(u,v) \in \mathcal{E}} \|\rho_{u \triangleleft e} \mathbf{h}_u - \rho_{v \triangleleft e} \mathbf{h}_v\|_2^2,$$

where $\rho_{u \triangleleft e} : \mathcal{F}(u) \rightarrow \mathcal{F}(e)$ and $\rho_{v \triangleleft e} : \mathcal{F}(v) \rightarrow \mathcal{F}(e)$ are linear restriction maps that project vertex representations into the edge-local coordinate system. The key insight is that these transformations break the uniform aggregation pattern of standard GNNs, allowing neighboring nodes to maintain distinct local representations even after multiple diffusion steps.

Sheaf Laplacian. The gradient of $\mathcal{E}_{\mathcal{F}}$ with respect to \mathbf{h} defines the sheaf Laplacian operator $\mathcal{L}_{\mathcal{F}}$. For a node u , this operator aggregates edge-aligned differences across all incident edges:

$$(3.6) \quad (\mathcal{L}_{\mathcal{F}} \mathbf{h})_u = \sum_{e:u \in e} \rho_{u \triangleleft e}^{\top} (\rho_{u \triangleleft e} \mathbf{h}_u - \rho_{v \triangleleft e} \mathbf{h}_v),$$

where the sum is taken over all edges $e = (u, v)$ incident to u . This formulation generalizes the standard graph Laplacian to vector-valued signals with heterogeneous local coordinate systems. The restriction maps act as learnable, edge-specific weights that modulate information flow based on local graph structure and node features. The generalization to higher-dimensional stalks and learnable restriction maps significantly expands the representational capacity of the diffusion process.

A critical design choice in sheaf neural networks is how to parameterize the restriction maps $\rho_{u \triangleleft e}$ and

$\rho_{v \triangleleft e}$. In principle, these could be arbitrary linear operators in $\mathbb{R}^{d \times d}$, but this would introduce $O(Ed^2)$ parameters, leading to substantial computational cost and overfitting risk, particularly for large graphs. We adopt a diagonal parameterization where each restriction map is represented as element-wise multiplication by a learned vector:

$$(3.7) \quad \rho_{u \triangleleft e} \mathbf{h}_u = \mathbf{r}_{u \triangleleft e} \odot \mathbf{h}_u,$$

where $\mathbf{r}_{u \triangleleft e} \in \mathbb{R}^d$ is a learnable diagonal vector and \odot denotes element-wise product. This reduces the parameter count from $O(Ed^2)$ to $O(Ed)$.

Learning restriction maps can be done statically, where they are computed once from fixed node embeddings and reused across all inputs, or dynamically, for graphs where edge semantics evolve based on node features. We adopt dynamic signal-conditioned restriction maps to be learned in the following way:

$$(3.8) \quad [\mathbf{r}_{u \triangleleft e}, \mathbf{r}_{v \triangleleft e}] = \text{MLP}(\mathbf{h}_u \parallel \mathbf{h}_v),$$

conditioned on the node representations at a given time step. This signal conditioning allows the sheaf structure to adapt based on the input, enabling the model to dynamically adjust information flow patterns. To stabilize training, we also apply a residual connection in restriction map computations with a small initialization:

$$(3.9) \quad \mathbf{r}_{u \triangleleft e} \leftarrow \mathbf{r}_{u \triangleleft e} + \alpha \cdot \text{MLP}_{\text{res}}([\mathbf{h}_u \parallel \mathbf{h}_v]),$$

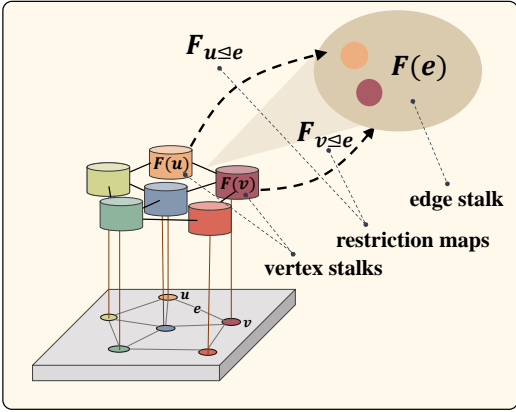


Figure 3.2: Sheaf graph representation with learned dynamic restriction maps. Each node is associated with a vertex stalk and each edge is associated with an edge stalk. Restriction maps define the relation between vertex stalks and edge stalks.

where $\alpha = 0.1$ is a scaling coefficient and MLP_{res} is initialized with near-zero weights. In our experiments, we find that dynamic signal-conditioned maps are essential for spatio-temporal forecasting tasks where edge semantics depend on current traffic conditions, weather patterns, or other time-varying factors.

To prevent high-degree nodes from dominating the diffusion process, we also perform degree-based normalization. Let $\text{deg}(u)$ denote the degree of node u . For each edge $e = (u, v)$, the normalization coefficient:

$$(3.10) \quad w_e = \frac{1}{\sqrt{\text{deg}(u) \cdot \text{deg}(v)}}.$$

This ensures that information from high-degree nodes is appropriately scaled during aggregation.

Sheaf diffusion. The process of sheaf diffusion (which is equivalent to heat diffusion over sheaf structures) facilitates a form of inter-dimensional information exchange that captures intricate relationships among nodes. Additionally, as the diffusion process converges, it strengthens the capacity to linearly separate node representations. For each edge $e = (u, v)$, we compute the sheaf-aligned discrepancy $\delta_e = (\mathbf{r}_{u \leq e} \odot \mathbf{h}_u) - (\mathbf{r}_{v \leq e} \odot \mathbf{h}_v)$. Messages are aggregated using a signed scatter operation:

$$(3.11) \quad \mathbf{m}_u = \sum_{e:\text{src}(e)=u} w_e \delta_e - \sum_{e:\text{dst}(e)=u} w_e \delta_e.$$

The message \mathbf{m}_u is transformed and combined with the original representation $\mathbf{h}_u^{(\ell)}$ via a residual connection and feed-forward network to produce a candidate update $\tilde{\mathbf{h}}_u$.

Crucially, a learnable gate then adaptively blends the original and updated representations:

$$(3.12) \quad \mathbf{g}_u = \sigma(\mathbf{W}_g^{(\ell)}[\mathbf{h}_u^{(\ell)} \parallel \tilde{\mathbf{h}}_u]), \quad \mathbf{h}_u^{(\ell+1)} = \mathbf{g}_u \odot \tilde{\mathbf{h}}_u + (1 - \mathbf{g}_u) \odot \mathbf{h}_u^{(\ell)}.$$

While residuals stabilize training in deep stacks, the gating mechanism enables feature-selective propagation to preserve discriminative node features when $\mathbf{g}_u \approx 0$ and allows more informative diffusion when $\mathbf{g}_u \approx 1$. After L diffusion layers, the final representations are decoded to forecasts $\hat{\mathbf{Y}} \in \mathbb{R}^{B \times H \times N \times F_{\text{out}}}$ via a linear projection.

4 Experimental Setup We conduct our experiments on six widely recognized real-world benchmark datasets commonly used for spatio-temporal forecasting. Firstly, the METR-LA dataset [21], which was collected from freeway networks in Los Angeles. This dataset has become a standard benchmark in the literature due to its rich temporal patterns and moderate spatial coverage. In addition, we include the PEMS04 and PEMS08 datasets [24], which originate from different regions within the Caltrans Performance Measurement System (PeMS) and provide further variability in graph topology and traffic flow dynamics. To further evaluate the robustness of our framework under complex urban traffic conditions, we also conduct experiments on the NAVER-Seoul dataset [20]. NAVER-Seoul covers the entire main road network in Seoul, South Korea, and features more abrupt fluctuations in traffic speed as well as a significantly larger number of sensors. This makes it a particularly challenging benchmark, well-suited for testing the scalability and generalization ability of spatio-temporal models. To examine the generalizability of our solution to other domains, we also run experiments on the Molene weather dataset, which was collected in the Brest region in France [12]. Moreover, we evaluate on the Air Quality dataset [22], which contains hourly measurements of the pollutant $PM_{2.5}$ collected by 437 air quality monitoring stations across 43 Chinese cities. A summary of the key characteristics of all datasets used in our experiments is provided in Table 3.1.

To ensure a fair and consistent evaluation, we adopt the same split data set as established in previous studies. Specifically, for the PEMS04 and PEMS08 datasets, we follow the 60:20:20 ratio of training, validation, and testing splits, as used in [24, 11, 26]. For the METR-LA and NAVER-Seoul datasets, we employ a 70:10:20 split, in line with the protocols outlined in [20, 21, 17], same for Molene and AirQuality datasets. Our experiments are conducted using the PyTorch framework, running on an NVIDIA GeForce RTX 4070 GPU with 8 GB of memory. Each experiment was repeated 3 times, and the average of the 3 is reported. We utilize Adam optimizer with an initial learning rate set to 0.01, a mini-batch

Table 3.1: Summary of datasets characteristics.

	METR-LA	NAVER-Seoul	PEMS04	PEMS08	Molene	AirQuality
Spatial Units	207	774	307	170	32	437
Timesteps	34,272	26,208	16992	17856	744	8760
Sampling Time	5 minutes	5 minutes	5 minutes	5 minutes	1 hour	1 hour
Start Time	03.2012	09.2020	01.2018	07.2016	01.2014	05.2014
End Time	06.2012	12.2020	02.2018	08.2016	01.2014	04.2015
Region	Los Angeles	Seoul	Bay Area	San Bernardino	Brest (France)	43 Chinese cities

size of 12 (to match sequence length), and the MAE loss function. We also employ early stopping based on the validation loss, with a patience threshold of 10 epochs. The model hyperparameters were selected empirically based on each dataset’s features. For smaller datasets, we select stalk dimension = 16, and for bigger datasets, we set it to 32. The number of diffusion layers was also selected in the same way, between 2 and 4. The range of temporal attention heads was selected between 4 and 8. All the exact numbers for each experiment are available in the code repository. Our evaluation metrics are: mean absolute error (MAE), root mean square error (RMSE), and mean absolute percentage error (MAPE). Missing values were excluded during the calculation of these metrics; the same procedure was followed in the baselines, too. We report all the evaluation metrics on traffic data to be consistent with previous works and select MAE for the weather and Air Quality datasets. Graph structures for each dataset are constructed using its pre-defined spatial adjacency matrices derived from the physical distances between station locations.

Each model is trained to forecast future timeseries conditions based on past temporal observations. Specifically, the input to the model consists of the previous 12 time steps in the case of the traffic dataset (METR-LA, NAVER-Seoul, PEMS04, PEMS08), which is equivalent to one hour of data, and 48 time steps in the case of the Air Quality, which is equivalent to 2 days, and 10 hours for the Molene dataset. The forecasting horizon in traffic is the same as the protocol established in all previous works: horizon 12 is one hour, horizon 6 is 30 minutes, and horizon 3 is 15 minutes. The same procedure for Molene (next 5 time steps) as in previous studies. Also for the Air Quality, the prediction is done on the next 48 hours, and we report the average of (1-12 h, 13-24 hr and 25-48 hr). To ensure consistent data scaling and improve convergence during training, we apply z-score normalization independently per sensor node across the dataset and then transform it back to its original form before evaluation. This is also consistent with the same procedure used in the baseline methods. Each component of our proposed framework, along with its associated hyperparameters, has been thoroughly exam-

ined through a series of experiments. To understand the individual contribution and sensitivity of each element, we conduct comprehensive ablation studies, the results of which are presented in the following section. We compare our proposed framework with the state-of-the-art models in spatio-temporal forecasting, selecting the top methods in each of the known methodological categories described in Section 2.

5 Results and Discussion

5.1 Overall Results Our evaluation across six datasets demonstrates that our framework achieves state-of-the-art or near-optimal performance across diverse forecasting horizons, domain characteristics, and environmental settings. Complete results are reported in Table 4.1 and Table 5.1. Several key observations emerge: First, traditional sequence-based methods such as ARIMA perform worst in most of the cases. This behavior is expected, as these methods ignore spatial connectivity and suffer severe degradation at long horizons. Second, GCN-based methods relying on uniform message passing exhibit competitive performance on medium-scale datasets but fail to generalize to large-scale heterogeneous data, such as NAVER-Seoul, where complex local dynamics dominate. In contrast, ST-Sheaf GNN demonstrates consistently strong performance, particularly on large-scale datasets with inherently complex spatio-temporal dynamics. Notably, ST-Sheaf exhibits the smallest performance degradation from short- to long-term forecasting horizons across all datasets. As shown in Figure 4.1, our framework avoids significant error accumulation at extended horizons, highlighting its robustness for long-term prediction.

Oversmoothing Experimental Analysis. Figure 5.1 illustrates a fundamental limitation of traditional GCNs that ST-Sheaf mitigates: rapid oversmoothing in deep architectures. We measure the average Euclidean distance between hidden representations of connected nodes at each layer during training on the Molene dataset. The GCN diffusion baseline (red curve) exhibits a catastrophic collapse of node representation diversity, with distances dropping below 1% of their initial Euclidean distance after only a few diffusion steps, rendering nodes

Table 4.1: Performance on NAVER-Seoul Dataset (South Korea) and METR-LA dataset (USA).

Data	Model	15min / horizon 3			30min / horizon 6			60min / horizon 12		
		MAE	RMSE	MAPE	MAE	RMSE	MAPE	MAE	RMSE	MAPE
NAVER-Seoul	ARIMA [21]	5.51	8.15	15.33	6.11	9.22	18.45	7.85	12.23	22.16
	STGCN [30]	4.63	6.92	14.49	5.50	8.83	17.37	6.77	10.89	20.42
	DCRNN [21]	4.86	7.12	15.35	5.67	8.80	18.38	6.40	10.06	21.09
	GW-Net [28]	4.91	7.24	14.86	5.26	8.13	16.16	5.55	8.77	16.97
	GMAN [32]	5.20	8.32	16.98	5.35	8.67	17.47	5.48	8.94	17.89
	ASTGCN [13]	5.09	7.44	16.14	5.71	8.73	18.78	6.22	9.58	20.37
	SGP [7]	4.87	7.28	15.63	5.48	8.61	18.12	6.01	9.64	20.04
	CITRUS [9]	5.29	7.80	16.78	6.17	9.56	20.20	7.16	11.31	24.10
	STDN [6]	4.73	6.82	14.46	5.12	7.95	16.12	5.94	9.02	18.01
ST-Sheaf (Ours)	4.52	6.60	14.23	5.01	7.72	16.06	5.11	8.32	16.91	
METR-LA	ARIMA [21]	3.99	8.21	9.60	5.15	10.45	12.70	6.90	13.23	17.40
	STGCN [30]	2.88	5.74	7.62	3.47	7.24	9.57	4.59	9.40	12.70
	DCRNN [21]	2.77	5.38	7.30	3.15	6.45	8.80	3.60	7.59	10.50
	GW-Net [28]	2.69	5.15	6.90	3.07	6.22	8.37	3.53	7.37	10.01
	GMAN [32]	2.86	5.77	7.76	3.14	6.59	8.73	3.48	7.35	10.10
	ASTGCN [13]	3.25	6.28	9.27	3.81	7.56	11.34	3.58	7.73	10.35
	SGP [7]	2.90	5.76	7.78	3.33	6.86	9.47	3.90	8.22	11.8
	CITRUS [9]	2.70	5.14	6.74	2.98	5.90	7.78	3.44	6.85	9.28
	STDN [6]	2.67	5.68	7.17	3.00	6.59	8.58	3.33	7.44	10.20
ST-Sheaf (Ours)	2.56	5.06	6.71	2.96	5.88	8.12	3.25	6.80	9.22	

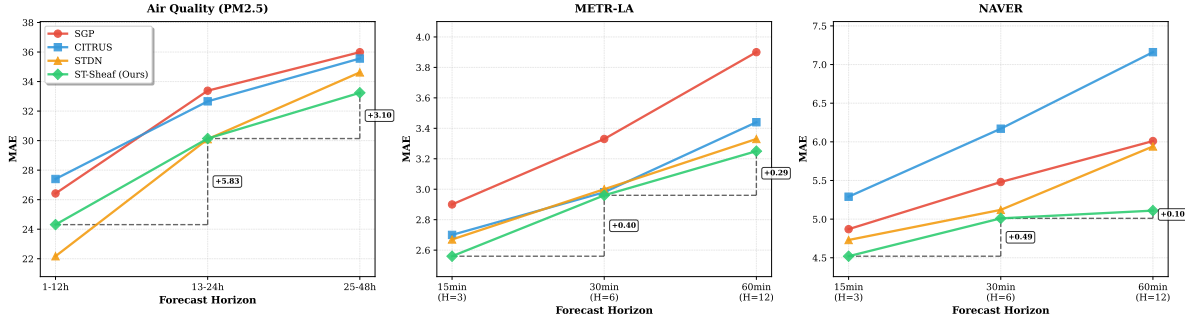


Figure 4.1: Forecasting error (MAE) across increasing prediction horizons on METR-LA, NAVER-Seoul, and Air Quality datasets. ST-Sheaf exhibits slower error accumulation over longer horizons compared to strong baselines.

Table 5.1: Performance on Molene weather dataset (France), Air Quality dataset (China) in MAE and PEMS04, PEMS08 traffic datasets (USA).

Model	Molene (weather)					Air Quality (PM2.5)			PEMS04			PEMS08		
	step-1	step-2	step-3	step-4	step-5	1-12 h	13-24 hr	25-48 hr	MAE	RMSE	MAPE	MAE	RMSE	MAPE
ARIMA [21]	0.445	0.750	1.041	1.327	1.592	30.14	38.98	44.10	33.73	48.80	24.18	31.09	44.32	22.73
STGCN [30]	1.066	1.552	1.933	2.225	2.698	22.77	31.59	35.59	22.70	35.55	14.59	18.02	27.83	11.40
DCRNN [21]	0.396	0.635	0.907	1.164	1.419	24.28	32.95	36.11	24.70	38.12	17.12	17.86	27.83	11.45
GW-Net [28]	0.855	1.124	1.455	1.865	2.104	22.42	30.29	34.73	25.45	39.70	17.29	19.13	31.05	12.68
GMAN [32]	0.962	1.424	1.882	2.022	2.417	24.11	32.80	36.25	20.23	32.17	17.06	16.47	25.72	10.48
ASTGCN [13]	0.981	1.342	1.877	1.906	2.125	25.51	33.98	37.42	22.80	35.82	16.56	18.63	28.27	13.08
SGP [7]	0.522	0.848	1.148	1.399	1.650	26.42	33.38	35.99	21.90	34.27	16.15	18.06	27.33	13.55
CITRUS [9]	0.497	0.757	1.048	1.332	1.600	27.40	32.66	35.56	22.64	35.08	16.83	17.89	27.81	11.21
STDN [6]	0.352	0.621	0.924	1.336	1.566	22.17	30.16	34.62	19.15	34.37	23.51	18.26	25.67	20.93
ST-Sheaf (Ours)	0.396	0.599	0.859	1.110	1.362	24.31	30.10	33.24	19.15	30.18	13.81	15.32	24.26	10.32

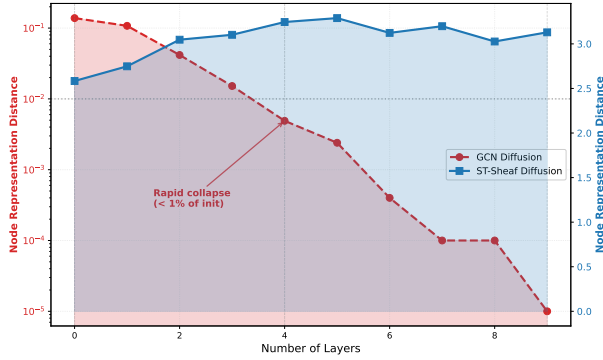


Figure 5.1: Oversmoothing Analysis: ST-Sheaf GNN diffusion vs. traditional GCN diffusion. The y-axis is the average Euclidean Distance of hidden representation between Connected nodes at each layer.

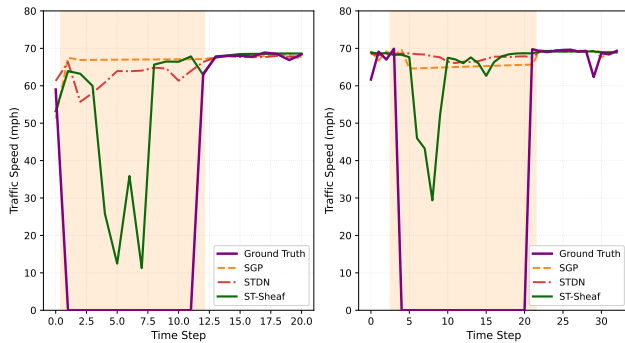


Figure 5.2: Case study of spatiotemporal dependency modeling on METR-LA test set: A congestion event originating at sensor 36 propagates to affect sensor 62 afterwards. The ST-Sheaf model captures this cascade effect in the prediction, while baseline methods fail to predict the induced slowdown.

effectively indistinguishable. This behavior explains the inability of standard GNNs to capture complex spatiotemporal dependencies beyond shallow networks. In contrast, ST-Sheaf maintains stable representation distances (blue curve) even with 10 layers, preserving node-specific discriminative information through its sheaf-based diffusion. By enforcing local consistency via restriction maps rather than global uniformity, the sheaf topology enables deep hierarchical modeling of heterogeneous higher-order relations that shallow networks cannot capture. These results empirically validate our central hypothesis that sheaf-based diffusion alleviates oversmoothing and supports deeper architectures.

We further present a case study on the METR-LA dataset in Figure 5.2. The left panel shows a congestion event at sensor 36, characterized by a sharp

drop in traffic speed, while the right panel illustrates its downstream impact on sensor 62. Strong recent baselines, including SGP (AAAI 2023), CITRUS (NeurIPS 2024), and STDN (AAAI 2025), fail to capture this cascaded dependency. In contrast, ST-Sheaf accurately models this cascaded event. This behavior highlights ST-Sheaf’s ability to dynamically adapt to evolving spatio-temporal conditions, making it well-suited for real-time management of complex systems.

Table 5.2 further highlights a key advantage of ST-Sheaf: parameter efficiency without sacrificing expressivity. While STDN contains nearly 6 million parameters, ST-Sheaf achieves superior forecasting performance with only 40 – 59k parameters, corresponding to a reduction of approximately 150 \times . Additionally, this efficiency does not compromise modeling capacity: ST-Sheaf’s parameters scale gracefully with graph size, increasing from 39.6K parameters at 170 nodes to 58.9K at 774 nodes. In contrast, STDN maintains a fixed parameter count of \sim 6M regardless of graph size, a clear indication of overparameterization that fails to adapt to problem scale. In terms of training efficiency, ST-Sheaf trains 4.0–5.6 \times faster per epoch than STDN and 2.8–4.0 \times faster than CITRUS across all datasets.

5.2 Ablation Studies We conduct comprehensive ablation studies to assess the contribution of individual mode components. Table 5.3 examines the effect of varying the sheaf stalk dimension d . Increasing d consistently improves performance, confirming that richer sheaf representations enhance model expressivity. However, these gains come with increased computational cost in terms of parameter count and training time. We observe diminishing returns beyond $d = 32$, where performance improvements no longer justify the efficiency tradeoff at very high dimensions. Accordingly, we set d between 16 and 32 in all experiments.

Table 5.4 reports the performance of several model variants. In the first variant, we replace dynamic restriction maps with static maps derived solely from graph topology, ignoring node states. This modification leads to performance degradation across all datasets, compared to the full model with dynamic maps, demonstrating that spatio-temporal systems exhibit time-varying structure that requires dynamic modeling. In the second variation, we remove the sheaf structure and diffusion entirely and replace them with standard GCN message passing. The resulting model reduces to temporal encoding combined with conventional graph convolutional layers. This variation exhibits substantial performance degradation, comparable to classic GCN-based baselines. In the third variation, we retain the sheaf topology and diffusion but remove the temporal encoding module, which is also important in capturing temporal dependencies. While this

Table 5.2: Number of model parameters and training time per epoch for different datasets (with different graph sizes to show how the model scales) compared to most recent SOTA: CITRUS (NeurIPS 2024), STDN (AAAI 2025).

Dataset (Graph Size)	CITRUS		STDN		ST-Sheaf	
	Time (s)	#Parameters	Time (s)	#Parameters	Time (s)	#Parameters
PEMS08 (N=170)	114.0	85,951	240.1	5,876,387	28.5↓	39,554↓
METR-LA (N=207)	114.1	86,743	419.6	5,971,107	40.9↓	40,738↓
PEMS04 (N=307)	116.2	90,335	649.3	6,227,107	53.2↓	43,938↓
NAVER-Seoul (N=774)	231.7	105,279	833.1	7,422,627	149.2↓	58,882↓

Table 5.3: Effect of stalk dimension (d) on performance and efficiency on Molene dataset, horizon 5, temporal heads=4, sheaf layers=2.

Stalk Dim	Epoch Time (s)	#Parameters	MAE
d=1	0.358	15490	1.533
d=4	0.369	17002	1.418
d=8	0.392	19410	1.378
d=16	0.453	25570	1.370
d=32	0.608	43266	1.362
d=64	0.864	100162	1.361
d=128	1.625	299970	1.360

Table 5.4: Ablation Studies on the effect of each of the model components on different datasets in MAE. For Molene, we select (step-1, 3, 5 as H1, H2, H3).

Dataset	Component	H1	H2	H3
METR-LA	Static restriction Maps	2.75	3.04	3.38
	W/o Sheaf Diffusion	3.05	3.57	4.44
	W/o Temporal Encoding	2.61	2.98	3.30
	ST-Sheaf (Full Model)	2.56	2.96	3.25
Molene	Static restriction Maps	0.44	0.92	1.46
	W/o Sheaf Diffusion	0.56	1.13	1.62
	W/o Temporal Encoding	0.41	0.88	1.39
	ST-Sheaf (Full Model)	0.39	0.85	1.36
AirQuality	Static restriction Maps	24.65	31.73	34.80
	W/o Sheaf Diffusion	27.88	34.21	36.72
	W/o Temporal Encoding	24.45	30.14	33.60
	ST-Sheaf (Full Model)	24.31	30.10	33.24

leads to a modest performance drop, the model still outperforms most baselines. This result indicates that sheaf diffusion and dynamic sheaf restriction maps account for the majority of the performance gain, while temporal encoding provides complementary improvements.

6 Conclusion We proposed ST-Sheaf, a novel spatio-temporal forecasting framework grounded in cellular sheaf theory that fundamentally rethinks information propagation across graph structures. By replacing uniform message passing with learned, dynamic restriction maps that adapt to local spatio-temporal contexts, ST-Sheaf captures asymmetric higher-order dependencies that are typically overlooked by conventional GNNs. Ex-

tensive experiments on six real-world benchmarks spanning traffic networks, weather systems, and air quality monitoring demonstrate that ST-Sheaf achieves state-of-the-art performance, with particularly pronounced gains in long-horizon forecasting where complex cascade effects are prominent. Our analysis shows that ST-Sheaf effectively models intricate spatio-temporal dependencies that strong baselines fail to capture, while also mitigating the oversmoothing phenomenon commonly observed in deep GNN architectures through sheaf-based diffusion. In addition, we observe consistent gains in computational efficiency. Beyond empirical performance, our work establishes sheaf theory as a principled mathematical foundation for spatio-temporal learning, opening new avenues for modeling complex systems with inherently non-stationary and context-dependent interactions. Promising future directions include extending sheaf diffusion to multimodal graphs and incorporating multi-relational sheaves for heterogeneous graph settings.

7 Reproducibility Statement We are committed to ensuring the reproducibility of our results. Detailed experimental setup and description of the datasets and data preprocessing steps are provided in Section 4. The code with appropriate documentation is available at: <https://anonymous.4open.science/r/ST-SheafGNN-6523/>.

References

- [1] Z. AL SAHLI AND M. AWAD, *Spatio-temporal graph neural networks: A survey*, arXiv e-prints, (2023), pp. arXiv-2301.
- [2] F. BARBERO, C. BODNAR, H. S. DE OCÁRIZ BORDE, AND P. LIO, *Sheaf attention networks*, in NeurIPS 2022 Workshop on Symmetry and Geometry in Neural Representations, 2022.
- [3] C. BODNAR, F. DI GIOVANNI, B. CHAMBERLAIN, P. LIO, AND M. BRONSTEIN, *Neural sheaf diffusion: A topological perspective on heterophily and oversmoothing in gnns*, Advances in Neural Information Processing Systems, 35 (2022), pp. 18527–18541.

- [4] C. BODNAR, F. FRASCA, Y. WANG, N. OTTER, G. F. MONTUFAR, P. LIO, AND M. BRONSTEIN, *Weisfeiler and lehman go topological: Message passing simplicial networks*, in International conference on machine learning, PMLR, 2021, pp. 1026–1037.
- [5] L. BRAITHWAITE, I. DUTA, AND P. LIÒ, *Heterogeneous sheaf neural networks*, arXiv preprint arXiv:2409.08036, (2024).
- [6] L. CAO, B. WANG, G. JIANG, Y. YU, AND J. DONG, *Spatiotemporal-aware trend-seasonality decomposition network for traffic flow forecasting*, in Proceedings of the AAAI Conference on Artificial Intelligence, vol. 39, 2025, pp. 11463–11471.
- [7] A. CINI, I. MARISCA, F. M. BIANCHI, AND C. ALIPPI, *Scalable spatiotemporal graph neural networks*, in Proceedings of the AAAI conference on artificial intelligence, vol. 37, 2023, pp. 7218–7226.
- [8] I. DUTA, G. CASSARÀ, F. SILVESTRI, AND P. LIÒ, *Sheaf hypergraph networks*, Advances in Neural Information Processing Systems, 36 (2023), pp. 12087–12099.
- [9] A. EINIZADE, F. MALLIAROS, AND J. H. GIRALDO, *Continuous product graph neural networks*, Advances in Neural Information Processing Systems, 37 (2024), pp. 90226–90252.
- [10] Y. FENG, J.-S. KIM, J.-W. YU, K.-C. RI, S.-J. YUN, I.-N. HAN, Z. QI, AND X. WANG, *Spatiotemporal informer: A new approach based on spatiotemporal embedding and attention for air quality forecasting*, Environmental Pollution, 336 (2023), p. 122402.
- [11] H. GAO, R. JIANG, Z. DONG, J. DENG, Y. MA, AND X. SONG, *Spatial-temporal-decoupled masked pre-training for spatiotemporal forecasting*, in Proceedings of the Thirty-Third International Joint Conference on Artificial Intelligence, 2024, pp. 3998–4006.
- [12] B. GIRAULT, *Stationary graph signals using an isometric graph translation*, in 2015 23rd European Signal Processing Conference (EUSIPCO), IEEE, 2015, pp. 1516–1520.
- [13] S. GUO, Y. LIN, N. FENG, C. SONG, AND H. WAN, *Attention based spatial-temporal graph convolutional networks for traffic flow forecasting*, in Proceedings of the AAAI conference on artificial intelligence, vol. 33, 2019, pp. 922–929.
- [14] J. HANSEN AND T. GEBHART, *Sheaf neural networks*, in NeurIPS Workshop on Topological Data Analysis and Beyond, 2020.
- [15] J. HANSEN AND R. GHRIST, *Toward a spectral theory of cellular sheaves*, Journal of Applied and Computational Topology, 3 (2019), pp. 315–358.
- [16] J. HANSEN AND R. GHRIST, *Opinion dynamics on discourse sheaves*, SIAM Journal on Applied Mathematics, 81 (2021), pp. 2033–2060.
- [17] R. JIANG, Z. WANG, J. YONG, P. JEPH, Q. CHEN, Y. KOBAYASHI, X. SONG, S. FUKUSHIMA, AND T. SUZUMURA, *Spatio-temporal meta-graph learning for traffic forecasting*, in Proceedings of the AAAI conference on artificial intelligence, vol. 37, 2023, pp. 8078–8086.
- [18] G. JIN, Y. LIANG, Y. FANG, Z. SHAO, J. HUANG, J. ZHANG, AND Y. ZHENG, *Spatio-temporal graph neural networks for predictive learning in urban computing: A survey*, IEEE transactions on knowledge and data engineering, 36 (2023), pp. 5388–5408.
- [19] D. JYOTISHI AND S. DANDAPAT, *An attentive spatio-temporal learning-based network for cardiovascular disease diagnosis*, IEEE Transactions on Systems, Man, and Cybernetics: Systems, 53 (2023), pp. 4661–4671, <https://doi.org/10.1109/TSMC.2023.3257022>.
- [20] H. LEE, S. JIN, H. CHU, H. LIM, AND S. KO, *Learning to remember patterns: Pattern matching memory networks for traffic forecasting*, in International Conference on Learning Representations, 2022.
- [21] Y. LI, R. YU, C. SHAHABI, AND Y. LIU, *Diffusion convolutional recurrent neural network: Data-driven traffic forecasting*, in International Conference on Learning Representations, 2018.
- [22] MICROSOFT RESEARCH, *Urban air*. <https://www.microsoft.com/en-us/research/project/urban-air/>, accessed 2026. Accessed: 2026-02-04.
- [23] Z. A. SAHLI AND M. AWAD, *Spatio-temporal graph neural networks: A survey*, arXiv preprint arXiv:2301.10569, (2023).
- [24] C. SONG, Y. LIN, S. GUO, AND H. WAN, *Spatio-temporal synchronous graph convolutional networks: A new framework for spatial-temporal network data forecasting*, in Proceedings of the AAAI conference on artificial intelligence, vol. 34, 2020, pp. 914–921.

- [25] J. SUK, L. GIUSTI, T. HEMO, M. LOPEZ, K. BARMAS, AND C. BODNAR, *Surfing on the neural sheaf*, in NeurIPS 2022 Workshop on Symmetry and Geometry in Neural Representations, 2022.
- [26] Y. WANG, Z. ZHANG, S. PI, H. ZHANG, AND J. PI, *Dual-gated graph convolutional recurrent unit with integrated graph learning (dg3l): A novel recurrent network architecture with dynamic graph learning for spatio-temporal predictions*, Entropy, 27 (2025), p. 99.
- [27] Z. WU, S. PAN, G. LONG, J. JIANG, X. CHANG, AND C. ZHANG, *Connecting the dots: Multivariate time series forecasting with graph neural networks*, in Proceedings of the 26th ACM SIGKDD international conference on knowledge discovery & data mining, 2020, pp. 753–763.
- [28] Z. WU, S. PAN, G. LONG, J. JIANG, AND C. ZHANG, *Graph wavenet for deep spatial-temporal graph modeling*, in 28th International Joint Conference on Artificial Intelligence (IJCAI-19), International Joint Conference on Artificial Intelligence (IJCAI), 2019.
- [29] Y. YANG, M. JIN, H. WEN, C. ZHANG, Y. LIANG, L. MA, Y. WANG, C. LIU, B. YANG, Z. XU, ET AL., *A survey on diffusion models for time series and spatio-temporal data*, CoRR, (2024).
- [30] B. YU, H. YIN, AND Z. ZHU, *Spatio-temporal graph convolutional networks: A deep learning framework for traffic forecasting*, in Proceedings of the Twenty-Seventh International Joint Conference on Artificial Intelligence, International Joint Conferences on Artificial Intelligence Organization, 2018, pp. 3634–3640.
- [31] O. ZAGHEN, A. LONGA, S. AZZOLIN, L. TELYATNIKOV, A. PASSERINI, AND P. LIO, *Sheaf diffusion goes nonlinear: Enhancing gns with adaptive sheaf laplacians*, in ICML 2024 Workshop on Geometry-grounded Representation Learning and Generative Modeling, 2024.
- [32] C. ZHENG, X. FAN, C. WANG, AND J. QI, *Gman: A graph multi-attention network for traffic prediction*, in Proceedings of the AAAI conference on artificial intelligence, vol. 34, 2020, pp. 1234–1241.